DESIGN AND MAGNETIC MEASUREMENT RESULTS OF THE HALF STORAGE RING MAGNETS*

T. H. Sun, H.-L. Xu†, B. Liu, G. Feng
University of Science and Technology of China, Hefei, China

Abstract

The Hefei Advanced Light Facility (HALF) is a fourth generation synchrotron light source under construction, centered on a 2.2 GeV diffraction limited storage ring (DLSR) with a design natural emittance below 86 pm·rad. The storage ring has a circumference of nearly 480 m and contains 880 magnets in 20 lattice cells, including longitudinal gradient bends (LGB), reverse bends (RB), quadrupoles (Q), sextupoles (S), octupoles (O), and all corrector magnets (CR). As of early 2026, all magnet types except the octupoles had completed series production and factory magnetic measurements. This paper presents the physical design methodology and key magnetic measurement results of the HALF storage ring magnets, and also outlines ongoing studies on Preisach hysteresis modeling and on magnetic crosstalk in selected compact magnet assemblies through three dimensional simulations and stretched wire measurements.

INTRODUCTION

HALF adopts a compact hybrid multi-bend achromat lattice to achieve ultralow emittance within a limited ring circumference [1], as shown in Fig. 1. Under this constraint, the storage ring magnets are densely packed, leading to short magnetic lengths for the multipole magnets. Meanwhile, to provide a relatively large good field region (13 mm) while maintaining high field quality (<0.05%), relatively large apertures are required [2]. The combination of short magnetic lengths and large apertures results in small aspect ratios, which enhance fringe field effects and make magnetic crosstalk between adjacent magnets non-negligible. These constraints increase the difficulty of magnet design and fabrication.

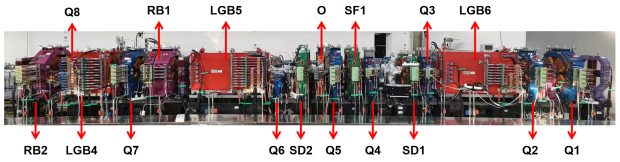

Figure 1: The lower half-cell of the HALF storage ring mockup, showing the compact arrangement of the main magnets. Corrector magnets are omitted for clarity.

To address these challenges, we established a magnet optimization workflow based on Gauss Newton algorithm (GNA) and Non-dominated Sorting Genetic Algorithm II (NSGA-II) and completed the physical design of the HALF storage ring multipole magnets [2]. Within the good field region, the designed multipole components of all magnets are better than 0.01%. Magnetic measurements obtained so far show that all magnets satisfy the physics requirements over their specified field or gradient tuning ranges.

The closed orbit of the storage ring is jointly provided by the longitudinal gradient bends and the reverse bends. By longitudinally redistributing the bending field, longitudinal gradient bends can suppress quantum excitation and reduce the beam equilibrium emittance. To accommodate a future energy upgrade of HALF to 2.5 GeV, an electromagnetic variable-gap concept was adopted for these magnets, offering more accurate and reproducible field tuning over a wide operating range than permanent magnets commonly used in fourth generation light sources [3]. Based on a design code based on the actual beam trajectory, all 123 longitudinal gradient bends in the storage ring, including three prototypes, have been fabricated and measured. The results confirm that the field homogeneity, trajectory control, and series consistency satisfy the design requirements.

The latter part of this paper also briefly discusses ongoing studies, including further investigations of magnetic crosstalk and hysteresis effects in magnets.

DESIGN AND MEASUREMENT RESULTS FOR HALF MAGNETS

Multipole Magnets

We developed a magnet optimization workflow based on the GNA and NSGA-II, as shown in Fig. 2. The workflow was implemented in MATLAB and coupled with OPERA for field evaluation during the optimization process [4,5]. GNA was used for magnets with relatively simple optimization objectives, whereas NSGA-II was introduced for cases requiring more stringent field quality optimization. To remain consistent with rotation coil measurements, the objective function was defined directly from the weighted multipole components normalized to the main field. For a quadrupole magnet, the objective function for pole shape optimization can be written as

$$F_Q = \sum_{m=1}^{4} W_m \, b_{2(2m+1)}^2, \qquad m = 1, 2, 3, 4.$$

In the geometric model, the initial pole shape was placed symmetrically on the positive semiaxis of the Y axis in a Cartesian coordinate system, and the profile perturbation was parameterized using a Legendre series. This parameterization helps preserve contour smoothness and suppress field quality degradation caused by local saturation. The

* This Work is supported by the National Nature Science Foundation of China under Grant No. 12075239.
† hlxu@ustc.edu.cn

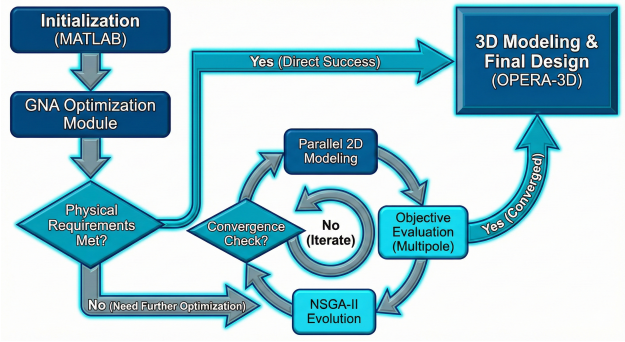

Figure 2: Optimization workflow for the multipole magnets.

perturbation was applied only to the Y coordinate, while the X coordinate remained unchanged. The displacement is given by

$$yvar_k = \sum_{l=1}^{L} \beta_l P_l\left(2 \times \frac{k-1}{K-1} - 1\right)$$

Here, P_l denotes the Legendre polynomial, L is the highest order, β_l is the relative coefficient, and K is the total number of points included in the optimization [6].

Magnetic measurements of the HALF storage ring multipole magnets were carried out using Hall probe and rotation coil methods. Except for the octupoles, all storage ring magnets have completed series production and passed factory magnetic acceptance measurements. The rotation coil measurements covered excitation curves, normalized multipole components, and magnetic center offsets.

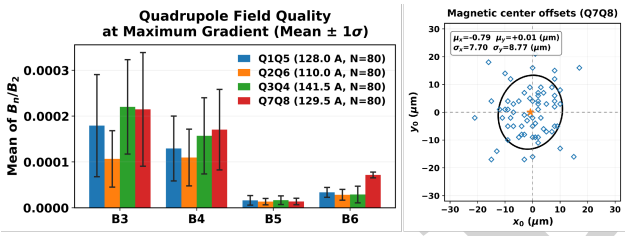

Figure 3: Multipole components of the quadrupoles at maximum gradient and the magnetic center offsets of Q7/Q8.

Table 1: Summary of field quality in reverse bends and sextupoles at maximum operating strength.

(a) Reverse bends: RB1 (100.8 A) and RB2 (96.6 A)

Order	Mean (RB1)	Std. Dev. (RB1)	Mean (RB2)	Std. Dev. (RB2)
B3	2.829×10^{-4}	1.238×10^{-4}	2.074×10^{-4}	9.771×10^{-5}
B4	1.018×10^{-4}	5.892×10^{-5}	6.857×10^{-5}	4.936×10^{-5}
B5	2.130×10^{-5}	1.431×10^{-5}	3.140×10^{-5}	5.451×10^{-6}
B6	8.293×10^{-6}	5.700×10^{-6}	1.235×10^{-5}	3.806×10^{-6}

(b) Sextupoles: SF1/SD2 (84.96 A) and SD1 (82.55 A)

Order	Mean (SF1/SD2)	Std. Dev. (SF1/SD2)	Mean (SD1)	Std. Dev. (SD1)
B4	3.657×10^{-4}	2.065×10^{-4}	3.431×10^{-4}	2.048×10^{-4}
B5	2.283×10^{-4}	1.320×10^{-4}	1.728×10^{-4}	1.004×10^{-4}
B6	5.532×10^{-5}	3.695×10^{-5}	5.143×10^{-5}	2.323×10^{-5}
B9	3.608×10^{-5}	2.017×10^{-5}	4.776×10^{-5}	2.022×10^{-5}

Figure 3 summarizes the multipole components of the quadrupole magnets at maximum gradient and shows the magnetic center offsets of Q7/Q8 as representative examples. The results indicate that the quadrupole field quality generally satisfies the design requirements. As the excitation enters the saturation region, slight magnetic center shifts are observed. The largest shift occurs in Q7/Q8 at maximum gradient, where the change relative to the magnetic center at the operating gradient is close to 12 μm. Table 1 summarizes the rotation coil results for the reverse bend magnets and sextupole magnets at maximum operating strength. For the sextupoles, the additional correction coils introduce extra multipole components and a slight attenuation of the main field. These effects were evaluated during the design stage and included in the error budget. At the maximum correction strength, the main sextupole field decreases by about 1%, and the difference between different correction paths is about 0.1%.

Longitudinal Gradient Bending Magnets

All longitudinal gradient bends in HALF adopt an electromagnetic variable-gap scheme to meet the field-tuning requirements of 2.2 GeV upgrade to 2.5 GeV. After the energy upgrade, the peak field will reach approximately 1 T; therefore, a moderate tapered expansion is introduced at the pole root to mitigate local magnetic saturation. Each magnet employs only a main coil and an auxiliary coil, with the auxiliary coil placed only on the pole with the highest field. In addition, the pole gap is treated as an adjustable parameter to improve the agreement between the measured and ideal field profiles (see Fig. 4). The results show that, with a pole gap machining tolerance of ±0.02 mm and a vertical assembly error of ±0.03 mm, the relative deviation between the measured and ideal field profiles remains below 0.3%. If the step fields were realized solely by adjusting the pole gap, the poles with lower fields would require significantly larger gaps, thereby enhancing the end fringe fields. Such a scheme is unacceptable in the compact storage ring layout of HALF.

With appropriate pole shape shimming and end chamfering, the longitudinal gradient bends achieved good field quality within the good field region. Based on Hall probe measurements on different vertical planes, the longitudinal integrated field homogeneity (see Fig. 5), the integrated field homogeneity along the actual trajectory, and the trajectory deviation were evaluated. The results show that the deviation of the actual trajectory from the ideal trajectory remains below 40 μm at all longitudinal positions. For batch-produced magnets, integral long coil measurements were used as the primary method for factory tests of field homogeneity and excitation curves, while Hall probe measurements served only

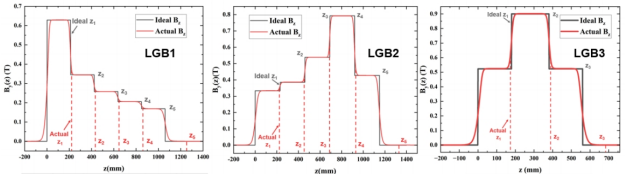

Figure 4: Longitudinal distributions of the vertical magnetic field for the three types of longitudinal gradient bends.

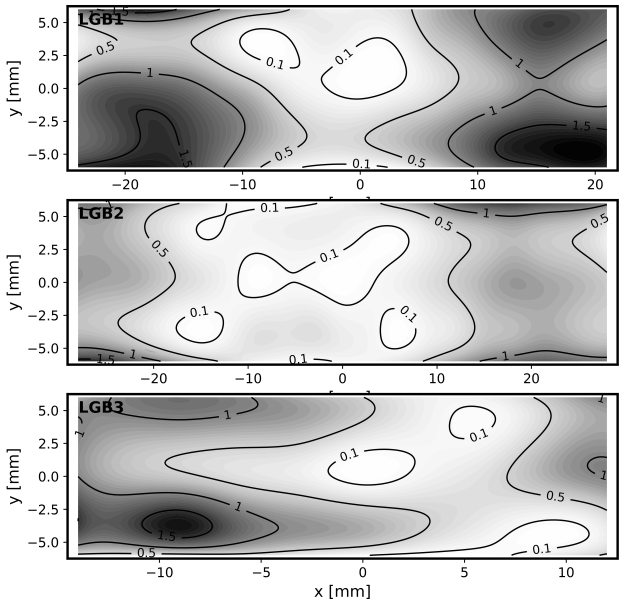

Figure 5: Contour maps of the longitudinal integrated field homogeneity for the prototypes of the three longitudinal gradient bends. The contour values are given in units of 10^{-4}.

as a supplementary tool for characterizing the longitudinal field distribution.

ONGOING STUDIES

Crosstalk Calculation and Measurement

The compact magnet layout in the HALF storage ring reduces the minimum spacing between adjacent main magnets to only 49 mm, making magnetic crosstalk unavoidable in practice. Crosstalk was analyzed using OPERA TOSCA after convergence tests. Here, we present only the representative Q4-SF1 case, which has been numerically analyzed and experimentally validated. When Q4 and SF1 operate simultaneously at their maximum gradients, the integrated gradient of Q4 is reduced by about 0.023%. As the SF1 current increases from zero to its maximum value, the relative reduction in the integrated gradient of Q4 decreases from about 0.06% to about 0.023%, indicating that crosstalk is significantly suppressed as the adjacent magnets enter saturation.

To validate the calculation, integrated field measurements of Q4 before and after the installation of SF1 were carried out using a stretched wire bench. After the installation of SF1, the simulated reduction in the integrated gradient of Q4 is about 0.06%, while the measured value is about 0.074%. The deviation among three repeated measurements is below 0.01%, and the difference between simulation and measurement is below 0.02%.

Hysteresis Effect

During storage ring commissioning, magnet operating points often move between the ascending and descending branches of the excitation loop. Because of hysteresis, the field produced by a magnet depends on both the instantaneous current and the excitation history [7] [8].

Using multi-path rotation coil data, we constructed a Preisach hysteresis model for the Q7/Q8 quadrupoles. The training set consists of two major loops of 0 A–150 A–0 A with current steps of 15 A and 7.5 A, and the prediction set is taken from a minor loop within 75 A $\pm$ 15 A. Because the HALF quadrupoles show weak hysteresis, narrow loops, and some saturation at high excitation, a seventh-order polynomial fitted to the midline of the ascending and descending branches of the major loop was used as the baseline, and the model was trained on the residual after baseline removal and normalization. Combined with two-stage optimization and smoothness constraints, the model shows improved stability and minor loop prediction capability. As shown in Fig. 6, the current implementation reproduces the overall trend of the minor loop, although further improvement in prediction accuracy is still needed.

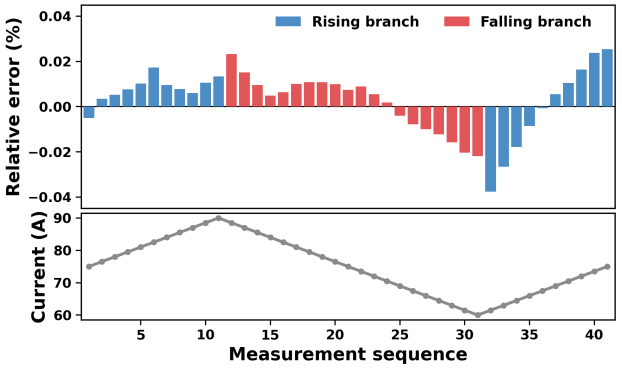

Figure 6: Relative prediction error of the minor loop and the corresponding excitation sequence. The upper panel shows the relative prediction error as a function of measurement sequence, and the lower panel shows the corresponding excitation current sequence.

CONCLUSION

In summary, this work has completed the physical design and magnetic measurements of the main magnets in the HALF storage ring. Except for the octupoles, all other magnet types have completed series production and factory magnetic measurements, and their overall performance satisfies the physics requirements. The longitudinal gradient bends meet the design targets in integrated field homogeneity, trajectory deviation, and series consistency. Numerical analysis and stretched wire measurements of magnetic crosstalk under the compact layout show good agreement, confirming the reliability of the evaluation method. Initial progress has also been achieved in Preisach hysteresis modeling for commissioning applications.

REFERENCES

[1] Z. Bai *et al.*, "A modified hybrid 6ba lattice for the half storage ring", in *Proc. IPAC'21*, Campinas, Brazil, May 2021, pp. 407–409. doi:10.18429/JACoW-IPAC2021-MOPAB112

[2] T. Sun *et al.*, "Status of multipole magnets for hefei advanced light facility", *IEEE Trans. Appl. Supercond.*, vol. 34, no. 5, pp. 1–6, 2024. doi:10.1109/TASC.2024.3355366

[3] T. Sun, X. Huang, Z. Zhang, B. Liu, Z. Ren, and H. Xu, "Status of longitudinal gradient bending magnets for hefei advanced light facility", *J. Instrum.*, vol. 20, no. 04, P04028, 2025. doi:10.1088/1748-0221/20/04/P04028

[4] The MathWorks, Inc., MATLAB VERSION: 24.2 (R2024B), 2024. https://www.mathworks.com

[5] Dassault Systèmes, SIMULIA OPERA, Dassault Systèmes, 2025. https://www.3ds.com/products/simulia/opera

[6] G. Le Bec, J. Chavanne, P. N'gotta, *et al.*, "Shape optimization for the esrf ii magnets", in *Proc. IPAC14*, Dresden, Germany, Jun. 2014, pp. 1232–1234. doi:10.18429/JACoW-IPAC2014-TUPRO082

[7] K.-H. Hoffmann and G. H. Meyer, "A least squares method for finding the preisach hysteresis operator from measurements", *Numerische Mathematik*, vol. 55, no. 6, pp. 695–710, 1989. doi:10.1007/BF01389337

[8] R. Roussel *et al.*, "Differentiable preisach modeling for characterization and optimization of particle accelerator systems with hysteresis", *Phys. Rev. Lett.*, vol. 128, no. 20, p. 204801, 2022. doi:10.1103/PhysRevLett.128.204801